Surface albedo as a proxy for land-cover clearing in seasonal dry forests: Evidence from the Brazilian Caatinga biome

[Updated version: 04 Dec 2018]

John Cunha[a, e, *], Rodolfo L. B. Nóbrega[b,c] , Iana Rufino[a], Stefan Erasmi[d], Carlos Galvao[a,e], Fernanda Valente[f]

[a]Federal University of Campina Grande, Center for Natural Resources and Technology, Campina Grande, Brazil;
[b]University of Reading, School of Archaeology, Geography and Environmental Science, Reading, United Kingdom;
[c]Imperial College London, Faculty of Natural Sciences, Department of Life Sciences, Ascot, United Kingdom;
[d]University of Gottingen, Institute of Geography, Cartography GIS & Remote Sensing Section, Goettingen, Germany;
[e]Griffith University, Cities Research Institute, Nathan Campus, Queensland 4111, Australia;
[f]University of Lisbon, School of Agriculture, Forest Research Centre (CEF), Tapada da Ajuda, 1349-017 Lisbon, Portugal.
*Corresponding author: john.brito@ufcg.edu.br

Abstract:

Ongoing increases in human and climate pressures, associated with the lack of monitoring initiatives, make the Caatinga one of the most vulnerable biomes in the world. The Caatinga is located in the semi-arid region of Brazil, and its vegetation phenology is highly dependent on precipitation, which has a high spatial and temporal variability. Under these circumstances, satellite image-based methods are valued due to their ability to uncover human induced changes from climate effects on land cover. In this study, a time series stack of 670 Landsat images over a period of 31 years (1985–2015) was used to investigate spatial and temporal patterns of land-cover clearing (LCC) due to vegetation removal in an area of the Caatinga biome. We compared the performance of surface albedo (SA), the Enhanced Vegetation Index (EVI) and the Normalized Difference Vegetation Index (NDVI) and evaluated their suitability for monitoring LCC in contrast to precipitation-related variations. We applied a residual trend analysis (TSS-RESTREND), with detection of significant structural changes (breakpoints) to monthly Landsat time series. Our results show that SA was able to identify LCC with a higher accuracy (89%) than EVI (44%) and NDVI (46%). The overall outcome of the study shows the benefits of using spectral indices of

Landsat time series that incorporate the short-wave infrared region, such as the SA, compared to vegetation indices for the monitoring of land-cover clearing, in seasonal dry forests such as the Caatinga.

Keywords: vegetation index; time series; Landsat; land-cover change; semi-arid.

1. Introduction

The identification of land-cover alteration driven by human action is one of the main challenges when studying seasonal dry forests (Yang et al., 2016; Wessels et al., 2007), being difficult to differentiate forest from non-forest areas (Mayes et al., 2015). In these areas, vegetation greenness is strongly related to the annual precipitation averages as well as the spatial variability and shifts of the rainy season period within a year (Hein et al., 2011). This effect of temporal and spatial climatic variability often masks the human actions in seasonal dry forests, especially after long drought periods (Zhang et al., 2014), because the dry vegetation sustains an extremely low level of photosynthetic material (Jacques et al., 2014), which is usually used as an indicator of changes in land cover of forests (Eckert et al., 2015; Tucker 1979; Xu et al., 2014). However, even under these circumstances, forests lose a very large proportion of the aboveground biomass when they are cleared (IPCC, 2000). The identification of changes in terrestrial forest biomass on annual basis is a prerequisite for improving estimates of terrestrial carbon sources (Le Toan et al., 2011), being the time-series analysis a widely accepted method to identify vegetation clearing (Song et al., 2014; Gómez et al., 2016).

Long time series of satellite data are suitable to assess vegetation dynamics on a regional scale (Schucknecht et al., 2013), being the Landsat data one of the most valuable sources of global observation. Owing to more than 30 years of medium-resolution and multispectral data, Landsat dataset constitute the longest continuous remotely-sensed record of the Earth's surface (Loveland and Dwyer, 2012). Despite its low temporal resolution at 16 days, earlier problems in images' absolute geolocation (Dwyer et al., 2018) and necessary adjustments of bidirectional reflectance effects (Egorov et al., 2018), Landsat imagery quality has improved. Landsat dataset structure provides information on radiometric, geometric and cloud cover quality to support temporal analysis (Wulder et al., 2016). The higher-level products are freely available by the United States Geological Survey (USGS) and allow users to retrieve surface reflectance data (Ju and Masek, 2016).

Trend analysis of indices based on visible and near-infrared (VIS-NIR, 0.4-1.1μm) wavelength ranges and computed from multi-year satellite data has been widely and successfully used to monitor changes in vegetation productivity (Fensholt et al. 2012; Higginbottom and Symeonakis, 2014; De Jong et al., 2012) and land degradation (Mariano et al., 2018; Li et al., 2016). On the other hand, the detection of land-cover clearing (LCC) in seasonal dry forests by using VIS-NIR, such as EVI and NDVI, is limited because of difficulties to distinguish deciduous vegetation from the underlying ground during dry period (Daughtry, 2001; Jacques et al., 2014; Mayes et al., 2015; Nagler et al., 2000; Xu et al., 2014). Zhao et al. (2018) highlight that while vegetation indices are routinely used to monitor ecosystem attributes and functions such as vegetation cover and primary productivity, the remote sensing-measured surface albedo (SA) can be used to assess ecosystem status in drylands. SA is more sensitive to changes in biomass (Rodríguez-Caballero et al., 2015); it has been used to monitor changes in dryland ecosystems and it is positively correlated with exposed soils (Yu et al., 2017), which are the outcome of the LCC process (Liu et al., 2016; Karnieli et al., 2014; Lamchin et al., 2016). SA is reported to be also sensitive to seasonal phenological variations (Wang et al., 2017; Samain et al., 2008), which are caused primarily by climatic variability in dry forests.

Different statistical approaches based on satellite data have been used to distinguish the effects of climatic variability on vegetation from anthropogenic actions on land cover in seasonal dry forests (Anyamba et al., 2014; DeVries et al., 2015; Evans and Geerken, 2004; Higginbottom and Symeonakis, 2014; Ibrahim et al., 2015; Karlson and Ostwald, 2016; Leroux et al., 2017; Verbesselt et al., 2016). In most of these studies, changes in the environment are identified by using trend analysis methods that remove the seasonal cycle within the time series. Here, we highlight two of them, considering their effectiveness to detect LCC in seasonal dry forests: the Break detection For Additive Season and Trend (BFAST, DeVries et al., 2015; Dutrieux et al., 2015; Verbesselt et al., 2012) and the RESidual TREND (RESTREND, Evans and Geerken, 2004; Li et al., 2016; Wessels et al., 2012) methods. To identify changes in land cover the BFAST method uses external regressors, which removes seasonal climatic effects on the analysed variable, such as the effects of rainfall on NDVI (De Jong et al., 2012). The RESTREND method is capable of coping with inter-annual rainfall variability and trends for detection of realistic levels of human-induced LCC (Wessels et al., 2012).

The TSS-RESTREND (Time Series Segmentation and RESidual TREND) method (Burrell et al., 2017) improves the BFAST and RESTREND analyses by attenuating seasonal climate effects (BFAST) and smoothing structural changes (breakpoints) due to rainfall variability. The Chow test (Chow, 1960) and the representation of the seasonal component by RESTREND are relevant mechanisms incorporated into TSS-RESTREND to overcome the limitations of the RESTREND and BFAST methods when each method is applied alone. The TSS-RESTREND method has two components: a structural change (breakpoint) detection and an overall trend estimation. While the first one is feasible to detect changes that occur abruptly, such as LCC, the latter is appropriate to identify trends that happen over a longer period of time.

In our study, we focus on the Caatinga biome, which is a seasonal dry forest constrained by climatic and anthropogenic pressures. Located in northeastern Brazil, a region dominated by a semi-arid climate with high temporal and spatial rainfall variability

(Marengo et al., 2017), the Caatinga vegetation is a heterogeneous (Rodal et al., 2008), seasonal semi-deciduous dry forest (Brito et al., 2012; Albuquerque et al., 2012), with its phenology driven by short-term rainfall patterns (Erasmi et al., 2014; Lima and Rodal, 2010). In this region, the human actions on the land cover have been related to the clearing of the vegetation, and typically occurred at small spatial scales, which can be better identified by using a higher spatial resolution (Lambin et al., 2003; Stroppiana et al., 2012). However, most vegetation studies that analyse long (> 30 years) remote sensing time series use vegetation indices at low spatial resolution, i.e., 1 to 8 km (Leroux et al., 2017), which is not sufficient to detect anthropogenic impacts on land cover at higher resolutions (Munyati and Mboweni, 2013) such as the ones in the Caatinga.

Our hypothesis was that the SA is a better indicator for LCC detection in seasonal dry forests, such as the Caatinga, than other vegetation indices, here represented by EVI and NDVI. Although the SA is known to show different responses between vegetated and bare soil surfaces, its use to identify LCC in dry forests has been poorly documented. We ascribe this scientific gap to the lack of global time-series datasets that provide multispectral data and to only recent developments on trend detection methods that translate the concept of abrupt LCC. In this study, this is addressed by using a 31-year spectral Landsat monthly time series applied to the TSS-RESTREND method in a Caatinga area that has been under an intense LCC process.

2. Study area and data

2.1. Study area

The study area is located in the Caatinga biome, which lies on the northeastern Brazil (Fig. 1A). The LCC in Caatinga is driven by the ways of living on the land (Andrade-Silva et al., 2012; Araújo et al., 2007, 2010; Santos and Tabarelli, 2002). Unlike most seasonal dry tropical forests that occur in isolated spots, the Caatinga biome spreads over a vast contiguous area, occupying ca. 830,000 km^2 (CNUC, 2017; Linares-Palomino et al., 2011). Although it is a unique ecosystem with a high degree of biodiversity and number of endemic species (Sobrinho et al., 2016), only 7.7% of its area is under environmental protection by the Brazilian National System of Conservation Units, which is 1.3% of restricted protection areas plus 6.4% of sustainable use areas (CNUC, 2017). The Caatinga is considered the most neglected and threatened Brazilian biome due to inadequate and unsustainable use of its natural resources over the past decades (Moro et al., 2016). Native vegetated areas of this biome have been cleared mainly because of ill-planned land use. In our study area, like many other parts of the Caatinga, this has been commonly characterized by LCC caused by wood removal for firewood/charcoal production (Leal et al., 2005; Sobrinho et al., 2016). Reforestation initiatives are rare in the Caatinga and recuperation of the Caatinga vegetation in cleared areas is a challenge because it may take several decades to naturally re-establish the original vegetation (Pereira et al., 2003; Araujo et al., 2007; Lima et al., 2016).

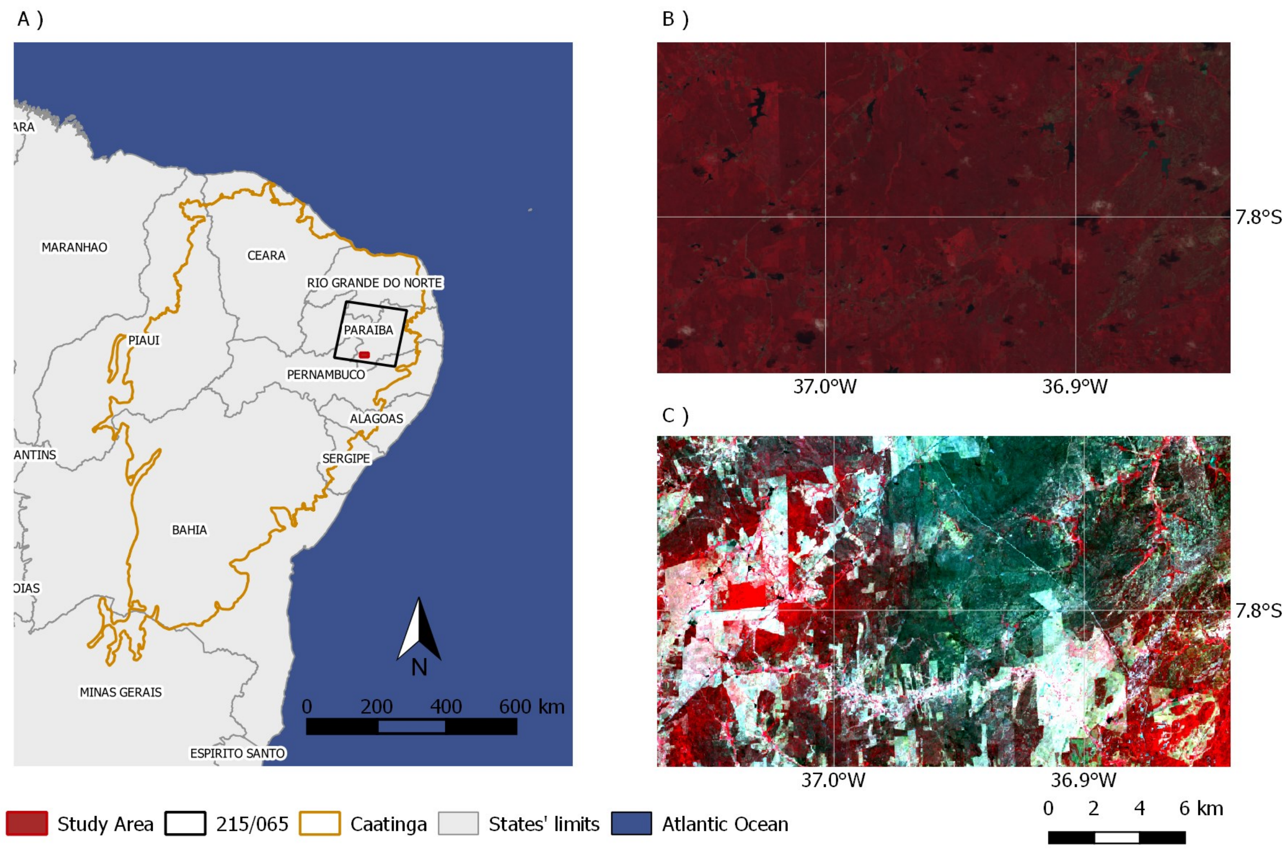

Fig. 1 - (A) Location of the Caatinga biome, Landsat scene 215/065 (path/row) and study area (Xmin: 37.07°W;

Xmax: 36.84ºW; Ymin: 7.86ºS; Ymax: 7.74ºS, WGS 84); (B) Landsat 5 false color composite (RGB to bands 4, 3 and 2) of the study area on 17/06/1984; (C) Landsat 8 false color composite (RGB to bands 5, 4 and 3) of the same area of (B) on 06/05/2015, showing land-cover differences between the first and last years of the studied period.

In this region, the main economic activities are livestock and subsistence farming (Belchior at al., 2017), leading to substantial LCC (Fig. 1B and C). The climate is hot semi-arid (BSh, Köppen classification) (Alvares et al., 2013), with only two distinct seasons: the very hot rainy season (from February to May) and the hot dry season (from June to January). The average annual rainfall in this region is approximately 550 mm, with high interannual variability (coefficient of variation of approximately 30%) and an average annual temperature of 23°C (Station code: 82792, INMET, 2018). The Standard Precipitation-Evapotranspiration Index (SPEI, Vicente-Serrano et al., 2010) for 12-month periods and the annual precipitation for the studied period and area are shown in Fig. 2. SPEI is a drought index based on the difference between precipitation and evapotranspiration that is usually used to detect and monitor drought periods. For the study area, the SPEI shows that the alternation between dry and wet periods have different magnitudes over the studied years.

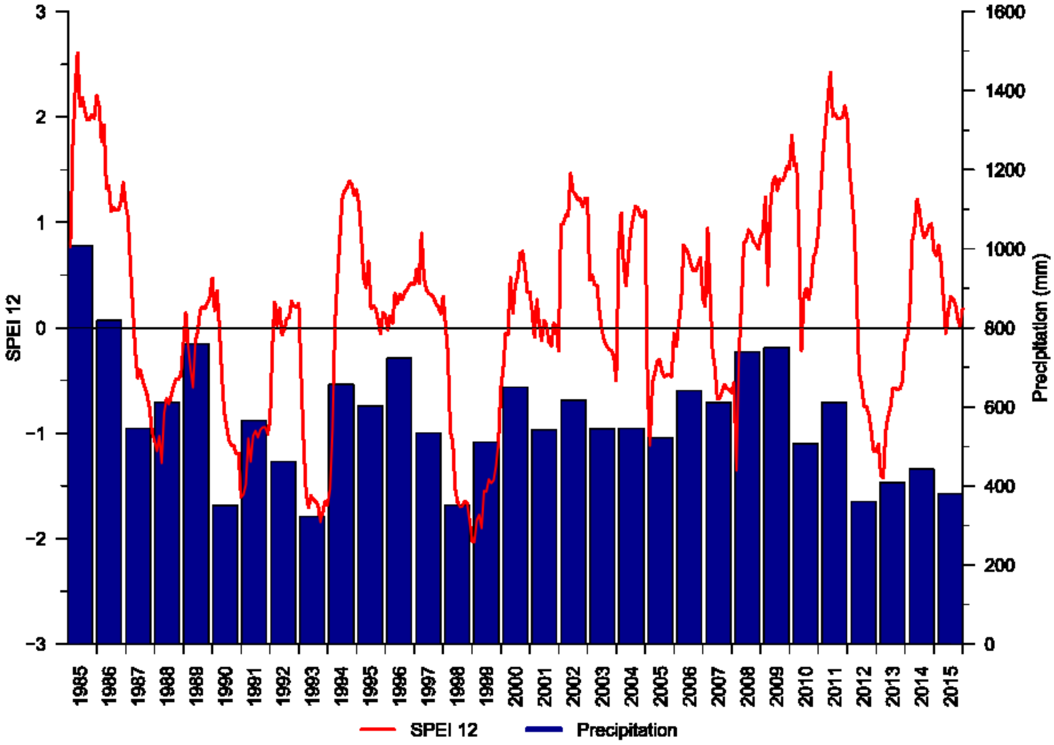

Fig. 2 - The 12-month Standardized Precipitation-Evapotranspiration Index - SPEI 12 (source: Beguería et al., 2017) and CHIRPS Precipitation (source: Funk et al., 2015) at geographic coordinates x: 36.75ºW, y: 7.75ºS, WGS 84.

2.2. Datasets

2.2.1. Landsat Surface Reflectance and Spectral indices

In this study, we used the atmospherically corrected surface reflectance (SR) from the Landsat satellites that are freely available by the United States Geological Survey (https://espa.cr.usgs.gov/). SR data are generated at 30-meter spatial resolution every 16 days. USGS provides the standard processing of SR including the Level 1 Standard Terrain Correction, resulting in ortho-rectified images of high geometric accuracy. Two different algorithms generates the SR data depending on the measuring sensor: for Landsat 5 TM and Landsat 7 ETM+ the SR data are obtained by the LEDAPS software (Masek et al., 2006), and for Landsat 8 OLI data are processed by the LaSRC algorithm (Vermote et al., 2016).

We identified 670 available Landsat images between 1985 and 2015 that cover our study area (390 from the TM sensor, 233 from the ETM+ and 47 from the OLI). For our analysis we used the Landsat Surface Reflectance Quality Assessment (pixel_qa band) to use only clear pixels (values 66 and 130 for Landsat 5 and 7, or 322 and 386 for Landsat 8, USGS, 2018a,b), which represented 46.8% of the total number of pixels.

The identification of LCC was obtained by using time series of NDVI (Tucker, 1979), EVI (Huete et al.,1997, 2002) and surface albedo (SA) (Shuai et al., 2014; Wang et al., 2016). For each Landsat image, NDVI, EVI and SA were calculated using Eqs. (1) to (3).

$$NDVI = \frac{\rho_{NIR} - \rho_{red}}{\rho_{NIR} + \rho_{red}} \quad (1)$$

$$EVI = 2.5 \times \frac{\rho_{NIR} - \rho_{red}}{\rho_{NIR} + 6 \times \rho_{red} - 7.5 \times \rho_{blue} + 1} \quad (2)$$

$$SA = b_{blue} \times \rho_{blue} + b_{green} \times \rho_{green} + b_{red} \times \rho_{red} + b_{NIR} \times \rho_{NIR} + b_{SWIR1} \times \rho_{SWIR1} + b_{SWIR2} \times \rho_{SWIR2} + b_0 \quad (3)$$

where ρ and b are the surface bidirectional reflectance values and their corresponding conversion coefficients for the six non-thermal Landsat bands, i.e., blue, green, red, NIR and the two shortwave infrared (SWIR1 and SWIR2) bands. Table 1 shows the b values of several spectral bands of the three satellites used in this study.

Table 1 - Band conversion coefficients used to calculate shortwave albedo for the different Landsat data.

Sensor	b_{blue}	b_{green}	b_{red}	b_{NIR}	b_{SWIR1}	b_{SWIR2}	b_0
Landsat-5 TM	0.3206	0	0.1572	0.3666	0.1162	0.0457	- 0.0063
Landsat-7 ETM+	0.3141	0	0.1607	0.3694	0.1160	0.0456	- 0.0057
Landsat-8 OLI	0.2453	0.0508	0.1804	0.3081	0.1332	0.0521	0.0011

The highest values of the vegetation indices are found in vegetated areas, while the lowest values occur in areas of bare soil (Mariano et al., 2018; Rodríguez-Caballero et al., 2015; Zhao et al. 2018). As SA has an inverse behaviour of vegetation indices, we used its complement to one (1 - SA) in the simulations, and thus ensuring a pattern of responses to LCC that corresponds to that of the vegetation indices EVI and NDVI.

To overcome the problem of clouds obstruction and temporal inconsistency in satellite time series, Holben (1986) presented a technique for the temporal composition of image time series. This method (Maximum Value Composite, MVC) uses the highest value for each pixel in a defined temporal segment (e.g. month, year). Although initially used only for NDVI with imagery of the Advanced Very High Resolution Radiometer (AVHRR) sensor, it has been successfully applied to other satellite sensors and indices (e.g., Huete et al., 2002). Flood (2013) showed that the medoid (a multi-dimensional analogue of the median) is a better measure to produce representative temporal image composites. In this study, we used the median to reduce the initial time series (SA, EVI and NDVI) to monthly composite images. Missing values were gap-filled by linear interpolation. Further, a linear Savitzky–Golay filter was applied (Chen et al., 2004; Savitzky and Golay, 1964), with a five-month half-width smoothing window, in order to reduce the noise caused by atmospheric variability.

2.2.1. Precipitation

The precipitation data used in this work were obtained from the Climate Hazards group InfraRed Precipitation with Stations (CHIRPS) dataset (Funk et al., 2015; Katsanos et al., 2016). CHIRPS is a near-global, very high spatial resolution (0.05° grid) precipitation product developed for monitoring environmental changes over land (Funk et al., 2015), which exhibited correlations ranging from 0.87 to 0.93 with rain gauge observations in the Caatinga (Paredes-Trejo et al., 2017). We used monthly precipitation data from October 1983 to December 2015.

3. Methods

3.1. TSS-RESTREND

The TSS-RESTREND method proposed by Burrell et al. (2017), combines the RESTREND technique (Evans and Geerken, 2004) and the BFAST methodology (Verbesselt et al., 2012, 2010), allowing a better and more accurate detection of structural changes in the ecosystems. Prior to the application of trend analysis, it is frequently necessary to remove the influence of exogenous random factors (e.g., rainfall, temperature) that, in addition to time and space, has a considerable effect on the response variable. The removal process, either by parametric (e.g., regression) or nonparametric (e.g., LOWESS) methods, reduces the variability of the studied variable and increases the power to detect changes in it (Helsel and Hirsch, 2002; Schertz et al., 1991). In remote sensing, a similar procedure has been applied for land-cover analysis. The RESTREND method analyzes the temporal trends in the vegetation precipitation relationship (VPR) residuals from a linear regression of the NDVI on the accumulated precipitation along a time period (Evans and Geerken, 2004). In Burrell et al. (2017), VPR is obtained for two sets of information: complete NDVI time series (CTS-NDVI) and annual maximum NDVI. In both cases, the linear regression uses the Optimal Precipitation Accumulated (OPA) calculated on a per-pixel basis, by an exhaustive search algorithm which combines different accumulation periods and lag times. The OPA used the CHIRPS precipitation data for accumulation periods of 1–12 months and lag times of 0–3 months, resulting in an increase of 15 months at the beginning of the precipitation series. The optimum VPR is established by finding the highest correlation coefficients between OPA and CTS-NDVI and between OPA and annual maximum NDVI.

TSS-RESTREND uses annual VPR to exclude pixels that do not meet the criteria to use the RESTREND method, i.e., a VPR that is significant, positive and consistent with time

(Wessels et al., 2012), and a gradual and consistent or monotonic residuals' trend (Jamali et al., 2015), and, then, applies BFAST to CTS-VPR residuals using the remaining pixels. The application of the BFAST method (Verbesselt et al., 2010) returns a list of potential breakpoints that are analyzed in a following step by the Chow test (Chow, 1960) to determine if there is a significant breakpoint. After identifying significant breakpoints, TSS-RESTREND calculates the significance of each identified change and identify the most significant breakpoint, if exists, as the structural change. For more details on the TSS-RESTREND method see Burrell et al. (2017).

In our study, TSS-RESTREND was applied using the TSS.RESTREND package for the R software environment (R Core Team, 2017). Although this method was initially used with NDVI data (Burrell et al., 2017), we additionally applied two spectral indices used study (SA and EVI) to one of the the component of this method that performs the structural change (breakpoint) detection. The original TSS.RESTREND package was adapted to receive raster files as input.

3.2. Validation Methodology

The performance of the TSS-RESTREND method was evaluated at both temporal and spatial levels. For each selected spectral indices and pixel, the year of the most significant breakpoint was registered and compared with the actual LCC year in order to evaluate the performance of SA, EVI and NDVI. The actual (true) year of LCC was determined by visual analysis of RapidEye images from 2015, which are freely available for academic use by the Brazilian Ministry of the Environment (http://geocatalogo.mma.gov.br/), Landsat images (false color composite) and satellite data from Google Earth Pro (https://earth.google.com/).

The validation dataset used in this work was built using a two-step procedure. First, a detailed visual survey of recent (2015) RapidEye images allowed the identification of several target areas where the original land cover had changed by the complete removal of the vegetation (land-cover clearing). Then, Landsat images and Google Earth Pro imagery was examined to determine the exact year of the LCC. Google Earth's historical imagery feature provided at least one cloud-free composite Landsat image per year for the study period and area at the altitude of visualization of 20 km. This satellite image time series allowed to establish the actual year of the clearing. Additionally, several places that had no visible human impact and that kept their original vegetation cover were chosen as validation pixels. In October 2017, there were field visits to the study area to confirm the land-cover status. Three different types of areas were included in the validation dataset (Fig. 3): 1) 45 target areas of 120 m buffer each (ca. 80 pixels), 31 exhibit LCC in the period 1985–2015 and 14 show a preserved natural vegetation; 2) a small region of 4.5 km^2 that has undergone a well-delimited time-space land-cover clearing process over the 2001–2012 period, hereafter referred to as "Subset I"; and 3) a region of 42 km^2 that has undergone a LCC process during 1985-2015, hereafter referred to as "Subset II".

For each of the 45 selected target areas, the areal median of each spectral index was calculated and the TSS-RESTREND was applied to the new generated time series. From its outcome, only the results from the structural change detection component were kept namely, the number of breakpoints, and the estimate and confidence interval of the date for each detected breakpoint (hereafter referred to as estimated LCC year). Based on the statistical theory proposed by Bai (1997), the breakpoints analysis implemented in the BFAST module (Verbesselt et al., 2010, Zeileis et al., 2002) calculates confidence intervals for the change-point date with less restrictive assumptions than those required by the usual parametric methods (i.e., independent and homogeneous normal errors). Due to these characteristics, these intervals were used in the validation of our results. The output of the TSS-RESTREND method was compared with the actual year of LCC and the accuracy of all indices was computed as the ratio of the number of target areas that were correctly estimated to the total number of target areas that actually belong to the following categories: a) *detected true*, when the actual LCC year was contained in the 95% confidence interval of the estimated LCC year; b) *time wrong*, when it did not lie in the 95% confidence interval; c) *false negative*, when the TSS-RESTREND method did not detect LCC, but it has actually occurred, and; d) *false positive*, when the TSS-RESTREND method detected a significant trend change on the spectral index in the time series but a LCC process did not occur. Three categories, i.e. detected true, time wrong and false negative, are related to the ability of detecting LCC when it actually took place, and the category false positive evaluate the efficiency of the method in verifying the lack of LCC.

The Subset I illustrates the process of fragmentation of land-cover clearing and the ability of the proposed methodology to identify these sequential changes. Within this area, pixels exhibiting land clearing in the same year were encompassed within the same patch. In addition, the median was calculated for the estimated LCC year of all pixels within each patch, providing a quantitative comparison with the actual year of change. The median rather than the mean was used as a summary measure because it is a robust statistic of central tendency, not influenced by extreme values (outliers). Additionally, the Kendall rank correlation coefficient (τ) between the median of the estimated LCC year and the actual vegetation clearing year for the nine patches was also calculated and its statistical significance tested. Subset II was used in a visual analysis between the estimate breakpoint dates detected by SA time series and Landsat images (false color composite) at 5-year intervals.

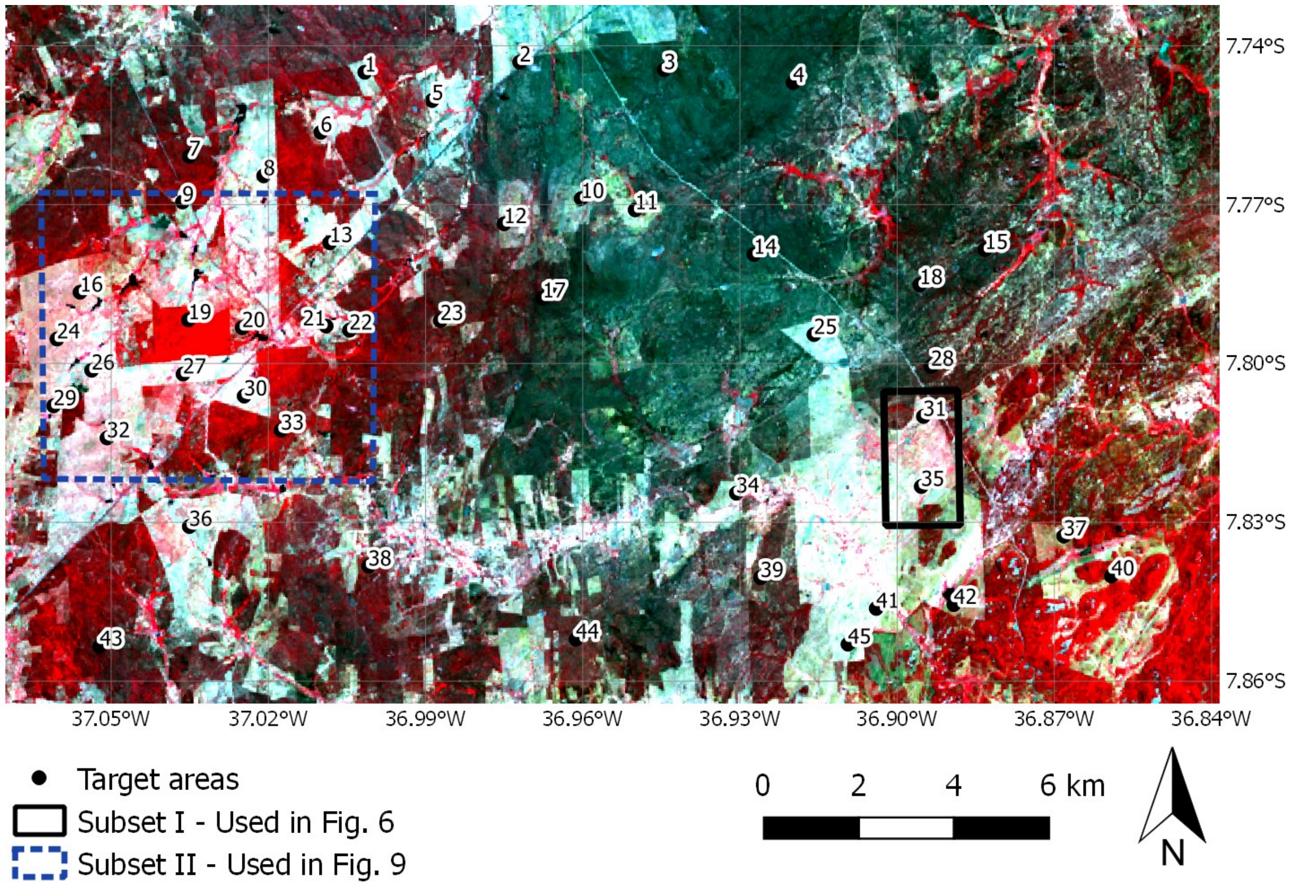

Fig. 3 - Location of the validation sites in the study area: 45 target areas (numbered, 31 target areas where a LCC actually occurred and 14 areas with preserved natural vegetation), the Subset I that had a sequential land-cover clearing process during 2001–2012 and the Subset II validation area. Source: Landsat 8 false color composite (RGB to bands 5, 4 and 3).

4. Results

Our analyses show that the two main differences between SA, and EVI and NDVI are (i) the range of values (Fig 4), (ii) the average number of breakpoints detected by the TSS-RESTREND method (Table 2). Whereas values ranged between 0.08 and 0.57 for EVI and 0.13 and 0.73 for NDVI, SA values varied only between 0.10 and 0.25. Moreover, the number of the breakpoints detected by using EVI and NDVI is greater than that with SA (Fig. 4). Most of the breakpoints occurred during a drought period (SPEI < -1, cf. Fig. 2), especially for EVI and NDVI.

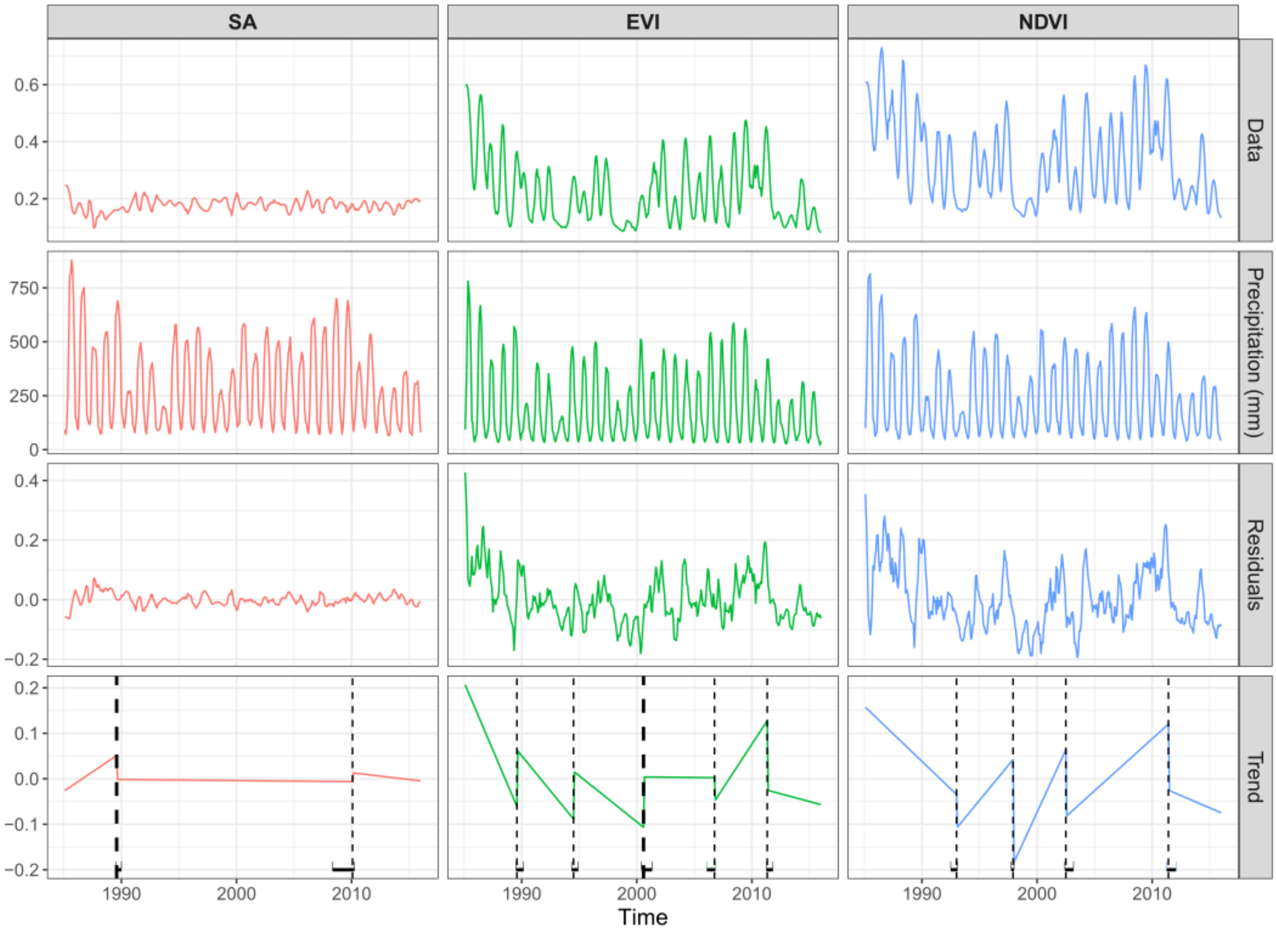

Fig. 4: TSS-RESTREND structural change detection outputs for the pixel at geographic coordinates x: 37.00445ºW, y: 7.79378ºS (target area 22). Top row panel shows SA, EVI and NDVI entire time series data, whereas the next painel has complete OPA time series, followed by monthly residuals of OPA, and Trend to each time series spectral indices. In the Trend panel, vertical lines represent breakpoints and the bold vertical line the most significative breakpoint.

In general, despite the smallest number of breakpoints identified by SA, this index showed the best performance in detecting LCC at annual scale and had on average the narrowest 95% confidence interval for the breakpoint date when compared to that of EVI and NDVI (Fig. 5, Table 2). The SA detected 89% of the LCC (being the sum of detected true and time wrong), while EVI and NDVI detected only 44% and 46%, respectively (Table 2). The low performance of EVI and NDVI is reflected by the great number of false negatives, representing 36–40%, whereas the false negatives were only 4% for SA . The total false positives represented over 15% for EVI and NDVI, and 7% for SA.

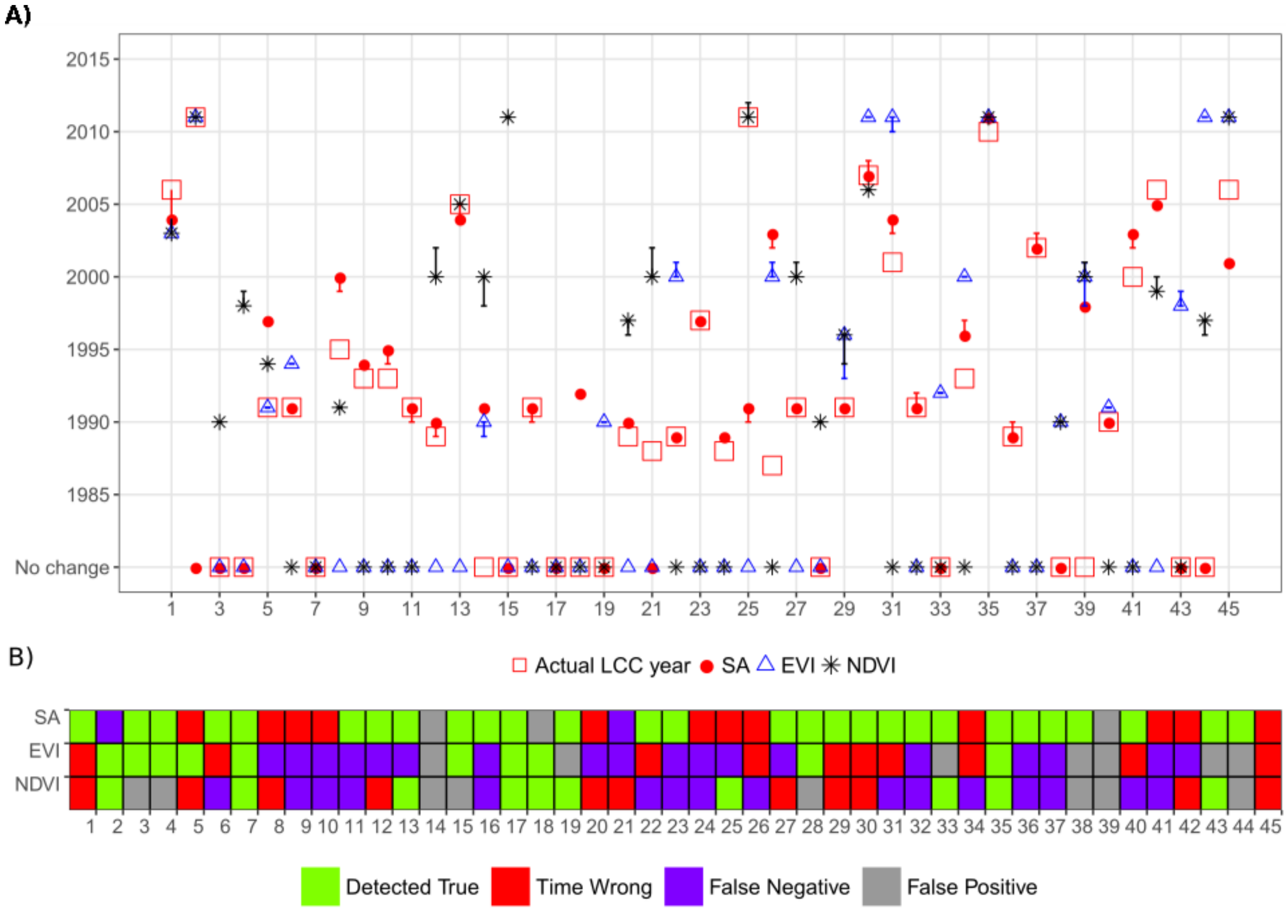

Fig. 5 – Estimated and actual year of land-cover clearing for SA, EVI and NDVI for the 45 target areas: A) Description and B) Summary

The subset I is a region with LCC between 2001 and 2012 (highlighted in Fig. 3 within the black polygon) and it was used to analyze the results in more detail (Fig. 6). This region contains two target areas, which exhibited contrasting performances: the LCC in the target area 31 was only detected by the SA, while the LCC for target area 35 was correctly detected by all three indices (Fig 5). Within the polygon, the main changes in land cover occurred between 2003 and 2012, which is shown by nine patches. Pixels within a same patch exhibit a similar actual LCC year. The analysis of these patches revealed that when EVI and NDVI were used a substantial number of pixels (sometimes > 40%) were categorized as false negative (Fig. 7A). This situation was particularly relevant in the patches where the LCC occurred in 2003, 2004, 2008 and 2010 (Fig. 6 and 7A). In contrast, results obtained with SA showed that false negative pixels were less than 10% for all patches (Fig. 7A) and exhibited an overall better accuracy in identifying the actual LCC year (Fig. 7B). In fact, for the nine patches the median of the estimated LCC year by SA was closer to the actual LCC year than those obtained with EVI and NDVI (Fig. 7B). This was also confirmed by Kendall's correlation coefficient (τ) between actual and estimated LCC years: SA had the highest value (τ = 0.86) with the highest significance ($p < 0.01$).

Table 2 – Number of validation target areas in the different categories (and percentage of the total) according to the results of the TSS-RESTREND method applied with the three spectral indices (Fig. 5), average confidence interval amplitude and average number breakpoint detected.

Index	Detected True	Time Wrong	False Positive	False Negative	Average 95% Confidence Interval amplitude (in months)	Average number of Breakpoints detected
SA	28 (62%)	12 (27%)	3 (7%)	2 (4%)	8.7	2.8
EVI	10 (22%)	10 (22%)	7 (16%)	18 (40%)	10.9	3.5
NDVI	10 (22%)	11 (24%)	8 (18%)	16 (36%)	11.6	4.0

The best performance of EVI and NDVI was observed for the patches where the clearing of vegetation took place in 2011 and 2012 (Figs. 6 and 7). However, for the other years and for a large number of pixels the estimated LCC year was around years of a severe drought (1993 and 2000, cf. Fig. 2). The foremost detected breakpoint years are the drought years of 1990 and 2000, and the period around 2010 (Fig. 7B and 8). Although there is a higher dispersion of the SA results than those of EVI and NDVI, the median of the detected year of change is closer to the observed date in the former index. Furthermore, while the validation polygon is hardly identified in the output raster of these two vegetation indices, it is quite well-defined in the SA raster (Fig. 6). This result is a consequence of the quite different performance of the TSS-RESTREND method to detect LCC when applied to time series of the three indices.

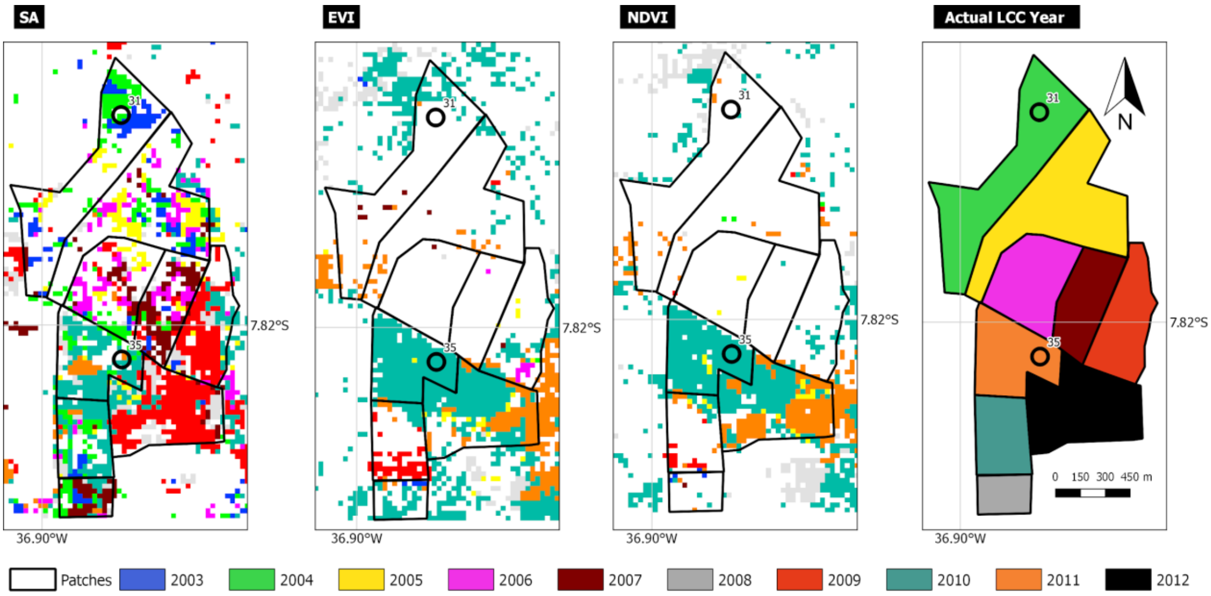

Fig. 6 – Polygon with selected patches showing the (a) detected breakpoint years of LCC for SA, EVI and NDVI, and (b) actual LCC year.

Visual comparison of the breakpoint raster for the subset II with Landsat images false color composite shows that the SA has some difficulty in identifying the correct year of clearing when it occurs during the initial and final years of the time series (1985–1990 and 2010–2015, Fig. 9). On the other hand, TSS-RESTREND and SA performed well for the small vegetation patches that remain unchanged during the study period (e.g., the regions between target areas 8–9 and 32–33).

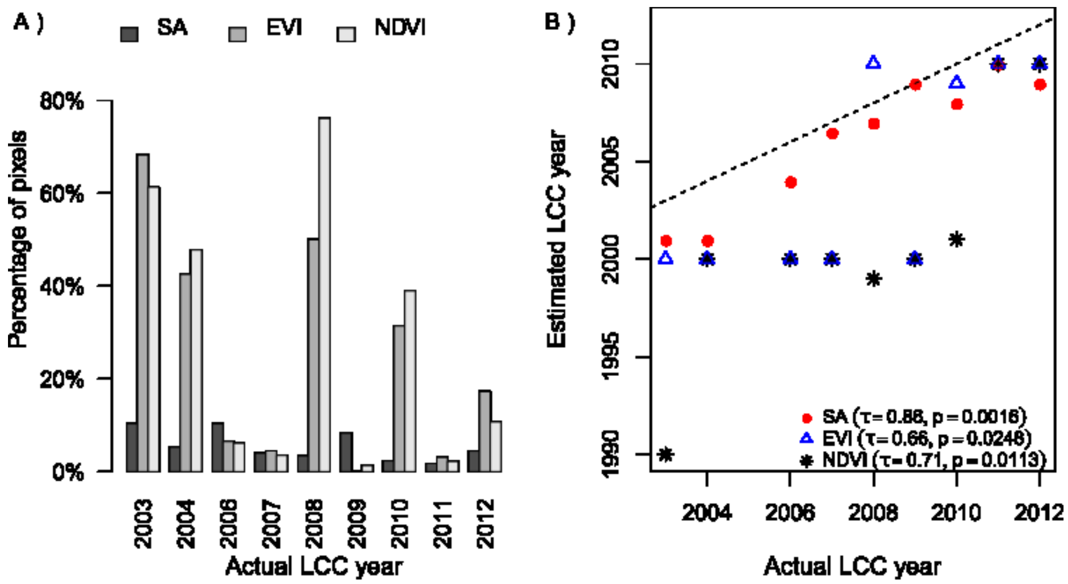

Fig. 7 - Observed change year of land-cover clearing of the different patches compared with the results obtained with the TSS-RESTREND method for the SA, NDVI and EVI: A) percentage of the total number of

pixels in each patch where the method output was classified as False Negative; B) median of the detected breakpoints within each of the nine patches for all the pixels where LCC was detected. The dotted line is the 1:1 line and □ is the Kendall rank correlation coefficient.

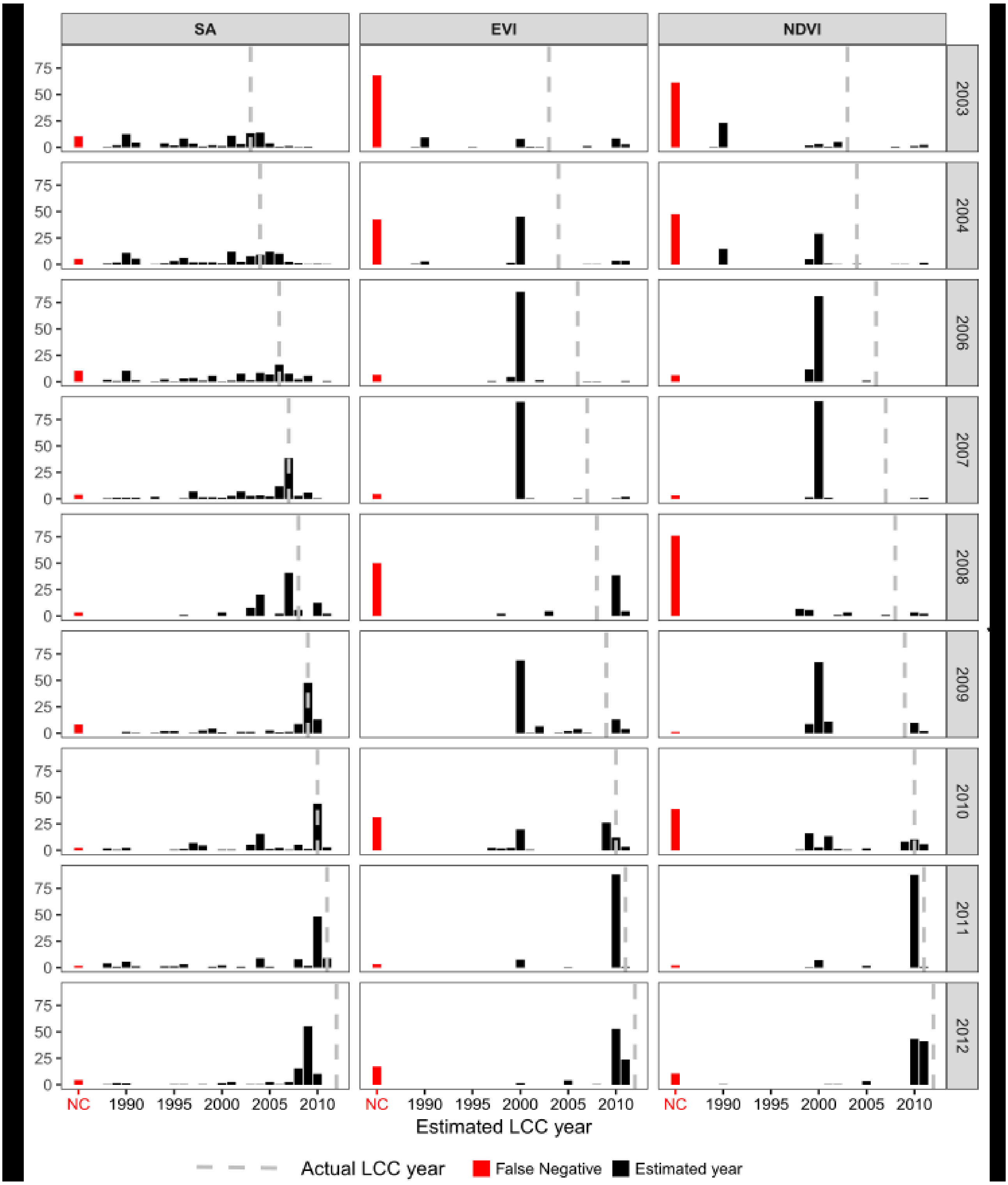

Fig. 8 – Bar plots of the detected breakpoint year obtained by the TSS-RESTREND method applied to the three spectral indices (SA, EVI and NDVI) for the different patches of the Subset I validation polygon. Each patch is identified by the year of the actual vegetation clearing (also marked by the grey dashed lines). The

height of each black bar is the percentage of pixels where a change was detected in that year. Red bars correspond to pixels where no change was detected.

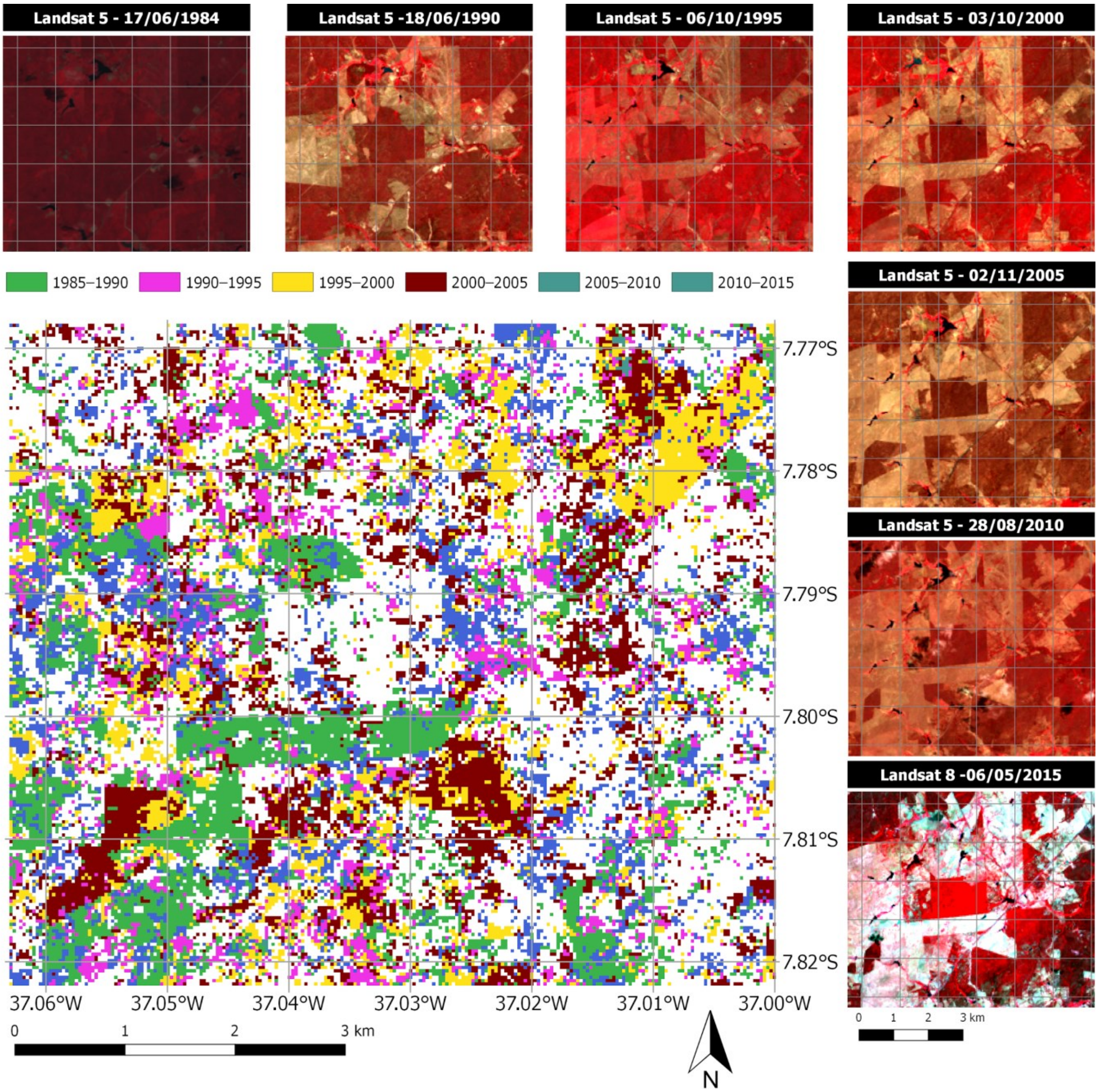

Fig. 9 - Estimated LCC year by the TSS-RESTREND method applied to the SA time series for the Subset II highlighted in Fig. 3. Images' source: Landsat 5 (RGB to 4, 3 and 2) and Landsat 8 (RGB to 5, 4 and 3) false color composite.

5. Discussion

Our study suggests that in the seasonal dry forests, especially the Brazilian Caatinga, neither EVI nor NDVI are reliable spectral indices for identifying LCC because of difficulties to distinguish deciduous vegetation from the underlying ground by indices that use the VIS–

NIR domain (Jacques et al., 2014; Mayes et al., 2015) during the dry period . Despite the wide acceptance of using EVI (Dutrieux et al., 2015) and NDVI (Leroux et al., 2017) to distinguish the effects of climate variability from anthropogenic actions on changes in land cover, these indices exhibited a low performance in detecting the correct timing of the LCC, as suggested by the TSS-RESTREND method. Furthermore, for EVI and NDVI a high number of false negatives (cf. Table 2, Figs. 6 and 7A), and the matching between actual and estimated LCC years were less than 25%, which is far from an acceptable standard for detecting changes in land cover (Aguirre-Gutiérrez et al., 2012; Mas, 1999).

The climate variability has a strong influence on EVI and NDVI in seasonal dry forests (Guan et al 2015; Walker et al, 2015). Despite the TSS-RESTREND method provides an approach to remove the effect of precipitation seasonality from the indices, these vegetation indices still show an effect due to extended drought periods. The years with the most severe droughts in the time series were 1990, 1993, 1998, and 2012. When the LCC occurred near to these years EVI and NDVI exhibited a circumstantial good efficiency in identifying LCC, which was the case in 1990 and, especially, 2012. While 2011 was a wet year (maximum SPEI > 2.4), 2012 was the beginning of an extremely dry period, under drought conditions (SPEI < -0.5) and with rainfall amounts below the total average (see Fig. 2).

SA exhibited a greater sensitivity to changes involving characteristics besides the greenness of leaves because this index covers other bands (SWIR 1 and SWIR 2) of the electromagnetic spectrum (Lui et al., 2017; Zhao et al., 2018), which are not used by indices that use VIS-NIR. When a soil-plant-atmosphere system is altered by an action of deforestation, the leafless woody biomass, which represents ca. 95% of the aboveground biomass in the Caatinga biome (Silva and Sampaio, 2008), is removed and consequently causing the total exposure of the soil to the effects of radiation, which can be detected by the SA. By contrast, we could not identify any pattern for the low performance in the detection of LCC for EVI and NDVI apart from the climate. For these two indices, the estimated LCC year is often confined into a moment near very dry periods. For example, 1990 was the first year with severe drought conditions in our time series, and it was the estimated LCC year by either EVI or NDVI for target points 3, 14, 19, 28 and 38, although no LCC actually occurred in these areas.

Since soil moisture has a high influence on SA, the spectral signals from dry and wet bare soil from a same site can be significantly different (He et al., 2014; Matthias et al., 2000). Therefore, the variation of SA values should be interpreted with caution when addressing LCC analysis. Like in most of the Caatinga region, the soils of our study area are shallow and present a low water storage capacity (Medeiros et al., 2018). When the land cover is cleared, the root zone storage is reduced, and, as a result, SA increases. However, in soils with greater depth and water retention capacities, SA may present lower performance as an indicator of LCC. Spectral indices that use the NIR and the SWIR bands also show a better ability to detect plant phenology than that of NDVI and EVI (Jin et al., 2013) by being more sensitive to the water content of vegetation and soil (Rodríguez-Caballero et al., 2015, Zhao et al., 2018). The spectral band SWIR provides a robust way to estimate the extent of bare soil and vegetation cover in arid and semi-arid regions (Asner and Lobell, 2000). Soil Tillage Index (STI), which uses SWIR domain, showed good performance to variance of dry masses in the Sahel (Jacques et al., 2014). DeVries et al. (2015) identified that the indices using the SWIR bands are more sensitive to LCC, especially the Tasseled Cap Wetness (TCW) index. The TCW index is defined on the same spectral bands used to calculate SA, which corroborates our results. We ascribe to soil moisture the cause of the errors in detecting the actual LCC year when using SA for the target areas 25 and 26. A substantial part of these two areas are covered by ephemeral stream beds, which despite exhibiting no surface water most of the years are known for acting as small aquifers by storing water in the alluvial deposits and increasing the soil moisture along stream channels (Fontes Junior and Montenegro, 2017).

The SA exhibited a high performance in detecting LCC (61%) or the lack of it (79%), totalling an overall accuracy of 89% for all 45 target areas. For the targets areas where the LCC was detected, 39% of them were time wrong and only 6% were false negatives. We attribute the imprecision in identifying the actual LCC year to some adverse effects of the ecosystem response to LCC on the SA. After vegetation removal, the remaining plant ecosystem, i.e., underground roots and soil, needs some time to adapt to the new conditions (Saco et al., 2018), which can cause a gradual loss of the root zone storage (D'Odorico et al., 2013), and, consequently, a delay in the full bare soil SA response, which in turn will cause a time wrong for the estimated LCC year that is after the actual one. Another aspect to consider is that some LCC activities in the Caatinga occurs at very small scales (e.g. activities on one-man farms) and they might overlap two consecutive years until the disturbance in the target's SA exceed a threshold that will qualify as breakpoint in the time series analysis (Pinheiro et al., 2013). We believe that the target areas 9, 10, 20 and 24 exhibit a 1-year delay for the detection of the actual LCC year. These four areas are located in the upper-left quadrant (see Fig. 3) and their LCC occured between 1988 and 1993, which was a period when this area was densely vegetated and its land cover was cleared after a highly fragmented LCC process (see Fig. 9). If this 1-year delay is added to the confidence interval of the estimated LCC years the rate of the time wrong rate is reduced from 39 to 26%. This is a decrease of 40% in the time wrong estimates, whereas the same 1-year delay tolerance only reduces 20% and 9% of EVI and NDVI time wrong LCC estimates, respectively.

The TSS-RESTREND method was built upon two previous approaches to the analysis of changes in land cover, i.e., BFAST and RESTREND, taking advantages of their individual skills in one robust method. Three main characteristics of the method were fundamental to the objective of selecting the best indicator of LCC in the Caatinga: the ability to (i) remove the influence in the process of the main climatic variable, the precipitation, (ii) detect, within the time series, structural changes in land cover, and (iii) select the most significant of such changes. The TSS-RESTREND, a method conceived, developed and validated to be used with vegetation indices, was evidenced as an efficient approach to be used with SA. The combination of the TSS-RESTREND and SA was appropriate to identify LCC in our Caatinga study area, where the clearing was followed by subsistence farming or livestock occupation with only few underbrush or grass that sustained the higher SA response, qualifying the clearing as the most significant breakpoint in the time-series analysis of the TSS-RESTREND. The slow reestablishment of native vegetation upon abandonment that maintain the bare soil exposed is due to the low natural fertility condition of the shallow and heterogeneous soils of the Caatinga (Salcedo et al., 1997; Sobrinho et al, 2016).

The two false negatives (in the target areas 2 and 21) detected by the SA represented areas that had their vegetation removed in either the first or last five years of the time series, i.e., 1985–1990 and 2010–2015. In these intervals, when using SA, the TSS-RESTREND method shows limitations in establishing a breakpoint. As in other time series analysis methods, errors at the beginning and at the end of any finite-length time series is a common issue (Torrence and Compo, 1998). The statistical theory that supports BFAST (Bai, 1997; Verbesselt et al., 2010), one of the main components of the TSS-RESTREND, requires that a minimum amount of data is set between successive breakpoints and at the beginning and at the end of the times series to be able to identify a structural change. Besides, the conclusion of a statistical hypothesis test (e.g., the Chow test) based on a small sample can be unreliable because the null hypothesis (corresponding to a non-significant breakpoint) will hardly be rejected at the standard significance levels. Therefore, the use of long time series is essential to reduce this type of uncertainties. In our study, most of the LCC occurred in the 1990s after the first five years of the time series. The Landsat dataset was a valuable source of information by providing long time series where these LCC processes could be evaluated free from these edge effects.

Our study supports further research towards a better understanding of Caatinga land-cover dynamics. Based on our work, further analysis and developments in this direction should consider: (i) a deep analysis of SA and other spectral bands applications in LCC studies in other seasonal tropical dry forests; (ii) a cross-related analysis of SA and other variables, such as biomass, evapotranspiration and soil moisture, supported by remote sensing data, and; (iii) the suitability of TSS-RESTREND components in identifying other type of land-cover change processes, such as degradation and fragmentation, not directly covered in our study.

6. Conclusions

We applied surface albedo, EVI and NDVI to the TSS-RESTREND method by using a 31-year Landsat time series to evaluate the performance of these indices to detect land-cover clearing in the Caatinga biome, a seasonal semi-deciduous tropical dry forest. We found that surface albedo exhibited a higher performance than the EVI and NDVI, and that the TSS-RESTREND was appropriate to identify the most significant structural change, which was the land-cover clearing.

The spatial resolution and long-term series of the Landsat images allowed a systematic assessment of altered targets on the land surface, laid out in a complex and fragmented pattern characteristic of the anthropogenic land-cover clearing in our studied area. TSS-RESTREND showed a satisfactory performance in using long-term satellite data to identify land-cover clearing in the Caatinga. The concept of this method is compatible with the reality of the land cover dynamics in this biome, since the selection of the most significant breakpoint unveils the land cover clearing without subsequent vegetation reestablishment. We found some imprecision in the method to identify land-cover clearing with false negative in the first and last few years of the time series (i.e., 1985–1990 and 2010–2015).

For the two different validation datasets used in this study (target areas and subset I), the surface albedo presented an overall better performance than NDVI and EVI, being able to detect land-cover clearing with an acceptable accuracy. The lower performance of the EVI and NDVI indices in the detection of land-cover clearing in the Caatinga biome is explained by their high sensitivity to leaf cover variations as a result of seasonal or extreme dry conditions. Changes in land cover affect the entire soil-plant-atmosphere system, such as removal of biomass and changes in soil properties, as well as in the microclimate, due to direct exposure to radiation, precipitation and wind. Based on those changes, studies should not rely only on vegetation indices but also look for other spectral ranges that will better represent the peculiar characteristics of specific ecosystems.

Acknowledgments

This work has been funded by the Brazilian National Council for Scientific and Technological Development (grant numbers 490115/2013-6 and 310789/2016-8) and the European Commission (grant number FP7-614048) through the EUBrazilCC project (http://eubrazilcloudconnect.eu/), CAPES-ANA (grant number 88887.115880/2015-01), and CAPES/PDSE (grant number 88881.134740/2016-01). This work also forms part of the UK/Brazil Nordeste project funded jointly through the UK Natural Environment Research Council (NE/N012526/1 ICL and NE/N012488/1 UoR) and the Fundação de Amparo à Pesquisa do Estado de São Paulo (2015/50488-5). The Forest Research Centre (CEF) is a research unit funded by Fundação para a Ciência e a Tecnologia I.P. (FCT), Portugal (UID/AGR/00239/2013).

References

Aguirre-Gutiérrez, J., Seijmonsbergen, A.C., Duivenvoorden, J.F., 2012. Optimizing land cover classification accuracy for change detection, a combined pixel-based and object-based approach in a mountainous area in Mexico. Appl. Geogr. 34, 29–37. doi:10.1016/j.apgeog.2011.10.010

Albuquerque, U.P., de Lima Araújo, E., El-Deir, A.C.A., de Lima, A.L.A., Souto, A., Bezerra, B.M., Ferraz, E.M.N., Maria Xavier Freire, E., Sampaio, E.V. de S.B., Las-Casas, F.M.G., de Moura, G.J.B., Pereira, G.A., de Melo, J.G., Alves Ramos, M., Rodal, M.J.N., Schiel, N., de Lyra-Neves, R.M., Alves, R.R.N., de Azevedo-Júnior, S.M., Telino Júnior, W.R., Severi, W., 2012. Caatinga Revisited: Ecology and Conservation of an Important Seasonal Dry Forest, The Scientific World Journal. doi:10.1100/2012/205182

Alvares, C.A., Stape, J.L., Sentelhas, P.C., De Moraes Gonçalves, J.L., Sparovek, G., 2013. Köppen's climate classification map for Brazil. Meteorol. Zeitschrift 22, 711–728. doi:10.1127/0941-2948/2013/0507

Andrade-Silva, A.C.R., Nemésio, A., de Oliveira, F.F., Nascimento, F.S., 2012. Spatial-Temporal Variation in Orchid Bee Communities (Hymenoptera: Apidae) in Remnants of Arboreal Caatinga in the Chapada Diamantina Region, State of Bahia, Brazil. Neotrop. Entomol. 41, 296–305. doi:10.1007/s13744-012-0053-9

Anyamba, A., Small, J.L., Tucker, C.J., Pak, E.W., 2014. Thirty-two Years of Sahelian Zone Growing Season Non-Stationary NDVI3g Patterns. Remote Sens. 6, 3101–3122. doi:10.3390/rs6043101

Araújo, E.L., Castro, C.C., Albuquerque, U.P., 2007. Dynamics of Brazilian Caatinga – A Review Concerning the Plants, Environment and People. Funct. Ecosyst. Communities 1, 15–28.

Araújo, V.F.P., Bandeira, a G., Vasconcellos, a, 2010. Abundance and stratification of soil macroarthropods in a Caatinga Forest in Northeast Brazil. Braz. J. Biol. 70, 737–46. doi:10.1590/S1519-69842010000400006

Asner, G. P., & Lobell, D. B. (2000). A Biogeophysical Approach for Automated SWIR Unmixing of Soils and Vegetation. Remote Sensing of Environment, 74(1), 99–112. doi:10.1016/s0034-4257(00)00126-7

Bai, J., 1997. Estimation of a Change Point in Multiple Regression Models. Rev. Econ. Stat. 79, 551–563. doi:10.1162/003465397557132

Begueria, S., Latorre, B., Reig, F., Vicente-Serrano, S.M. 2017. Global SPEI database. http://spei.csic.es/database.html. Access in 11 January 2017.

Belchior, M., Tai, D.W., Held, F.C. Von, 2017. Indicadores IBGE. Inst. Bras. Geogr. E Estatística - Ibge 6.

Brito, A.F., Presley, S.J., Santos, G.M.M., 2012. Temporal and trophic niche overlap in a guild of flower-visiting ants in a seasonal semi-arid tropical environment, Journal of Arid Environments. doi:10.1016/j.jaridenv.2012.07.001

Burrell, A.L., Evans, J.P., Liu, Y., 2017. Detecting dryland degradation using Time Series Segmentation and Residual Trend analysis (TSS-RESTREND). Remote Sens. Environ. doi:10.1016/j.rse.2017.05.018

Chen, J., Jönsson, P., Tamura, M., Gu, Z., Matsushita, B., Eklundh, L., 2004. A simple method for reconstructing a high-quality NDVI time-series data set based on the Savitzky-Golay filter. Remote Sens. Environ. 91, 332–344. doi:10.1016/j.rse.2004.03.014

Chow, G.C., 1960. Tests of equality between sets of coefficients in two linear regressions. Econometrica 28:591–605. doi:10.2307/1910133.

CNUC - Cadastro Nacional de Unidades de Conservação (Brazilian National Database of Conservation Units). Accessed in oct-2018

D'Odorico, P., Bhattachan, A., Davis, K.F., Ravi, S., Runyan, C.W., 2013. Global desertification: Drivers and feedbacks. Adv. Water Resour. 51, 326–344. doi:10.1016/j.advwatres.2012.01.013

Daughtry, C.S.T., 2001. Discriminating Crop Residues from Soil by Shortwave Infrared Reflectance. Agron. J. 93, 125. doi:10.2134/agronj2001.931125x

De Jong, R., Verbesselt, J., Schaepman, M.E., de Bruin, S., 2012. Trend changes in global greening and browning: Contribution of short-term trends to longer-term change. Glob. Chang. Biol. doi:10.1111/j.1365-2486.2011.02578.x

DeVries, B., Verbesselt, J., Kooistra, L., Herold, M., 2015. Robust monitoring of small-scale forest disturbances in a tropical montane forest using Landsat time series. Remote Sens. Environ. doi:10.1016/j.rse.2015.02.012

Dutrieux, L.P., Verbesselt, J., Kooistra, L., Herold, M., 2015. Monitoring forest cover loss using multiple data streams, a case study of a tropical dry forest in Bolivia. ISPRS J. Photogramm. Remote Sens. doi:10.1016/j.isprsjprs.2015.03.015

Dwyer, J., Roy, D., Sauer, B., Jenkerson, C., Zhang, H., Lymburner, L., 2018. Analysis Ready Data: Enabling Analysis of the Landsat Archive 1–24. doi:10.20944/PREPRINTS201808.0029.V1

Eckert, S., Hüsler, F., Liniger, H., Hodel, E., 2015. Trend analysis of MODIS NDVI time series for detecting land degradation and regeneration in Mongolia. J. Arid Environ. 113, 16–28. doi:10.1016/j.jaridenv.2014.09.001

Egorov, A. V., Roy, D.P., Zhang, H.K., Hansen, M.C., Kommareddy, A., 2018. Demonstration of percent tree cover mapping using Landsat Analysis Ready Data (ARD) and sensitivity with respect to Landsat ARD processing level. Remote Sensing 10. doi:10.3390/rs10020209

Erasmi, S., Schucknecht, A., Barbosa, M.P., Matschullat, J., 2014. Vegetation greenness in northeastern brazil and its relation to ENSO warm events. Remote Sens. 6, 3041–3058. doi:10.3390/rs6043041

Evans, J., Geerken, R., 2004. Discrimination between climate and human-induced dryland degradation. J. Arid Environ. 57, 535–554. doi:10.1016/S0140-1963(03)00121-6

Fensholt, R., Langanke, T., Rasmussen, K., Reenberg, A., Prince, S.D., Tucker, C., Scholes, R.J., Le, Q.B., Bondeau, A., Eastman, R., Epstein, H., Gaughan, A.E., Hellden, U., Mbow, C., Olsson, L., Paruelo, J., Schweitzer, C., Seaquist, J., Wessels, K., 2012. Greenness in semi-arid areas across the globe 1981-2007 - an Earth Observing Satellite based analysis of trends and drivers. Remote Sensing of Environment. 121, 144–158. doi:10.1016/j.rse.2012.01.017

Matthias, A.D.D., Fimbres, A., Sano, E.E.E., Post, D.F.F., Accioly, L., Batchily, A.K.K., Ferreira, L.G.G., 2000. Surface roughness effects on soil albedo. Soil Sci. Soc. Am. J. 64, 1035–1041. doi:10.2136/sssaj2000.6431035x

Flood, N., 2013. Seasonal composite Landsat TM/ETM+ Images using the medoid (a multi-dimensional median). Remote Sens. 5, 6481–6500. doi:10.3390/rs5126481

Fontes Júnior, R.V. de P., Montenegro, A.A. de A., 2017. Temporal dependence of potentiometric levels and groundwater salinity in alluvial aquifer upon rainfall and evapotranspiration. Rbrh 22. doi:10.1590/2318-0331.0217170059

Funk, C., Peterson, P., Landsfeld, M., Pedreros, D., Verdin, J., Shukla, S., Husak, G., Rowland, J., Harrison, L., Hoell, A., Michaelsen, J., 2015. The climate hazards infrared precipitation with stations—a new environmental record for monitoring extremes. Sci.

Data 2, 150066. doi:10.1038/sdata.2015.66

Gómez, C., White, J.C., Wulder, M.A., 2016. Optical remotely sensed time series data for land cover classification: A review. ISPRS Journal of Photogrammetry and Remote Sensing. doi:10.1016/j.isprsjprs.2016.03.008

Guan, K., Pan, M., Li, H., Wolf, A., Wu, J., Medvigy, D., Caylor, K.K., Sheffield, J., Wood, E.F., Malhi, Y., Liang, M., Kimball, J.S., Saleska, S.R., Berry, J., Joiner, J., Lyapustin, A.I., 2015. Photosynthetic seasonality of global tropical forests constrained by hydroclimate. Nat. Geosci. 8, 284–289. doi:10.1038/ngeo2382

He, C., Tian, J., Gao, B., Zhao, Y., 2015. Differentiating climate and human-induced drivers of grassland degradation in the Liao River Basin, China. Environ. Monit. Assess. 187, 4199. doi:10.1007/s10661-014-4199-2

Hein, L., De Ridder, N., Hiernaux, P., Leemans, R., De Wit, A., Schaepman, M., 2011. Desertification in the Sahel: Towards better accounting for ecosystem dynamics in the interpretation of remote sensing images. Journal of Arid Environments. 75, 1164–1172. doi:10.1016/j.jaridenv.2011.05.002

Helsel, D.R., Hirsch, R.M., 2002. Trend Analysis. Stat. Methods Water Resour. Tech. Water Resour. Investig. B. 4, chapter A3 323–355.

Higginbottom, T.P., Symeonakis, E., 2014. Assessing land degradation and desertification using vegetation index data: Current frameworks and future directions. Remote Sens. 6, 9552–9575. doi:10.3390/rs6109552

Holben, B.N., 1986. Characteristics of maximum-value composite images from temporal AVHRR data. Int. J. Remote Sens. 7, 1417–1434. doi:10.1080/01431168608948945

Huete, A., Didan, K., Miura, T., Rodriguez, E.P., Gao, X., Ferreira, L.G., 2002. Overview of the radiometric and biophysical performance of the MODIS vegetation indices. Remote Sens. Environ. 83, 195–213. doi:10.1016/S0034-4257(02)00096-2

Huete, A.R., Liu, H.Q., Batchily, K., J., L. van W., 1997. A comparison of vegetation indices over a global set of TM images for EOS-MODIS. Remote Sensing of Environment, 59(3), 440–451. doi:10.1016/s0034-4257(96)00112-5.

Ibrahim, Y.Z., Balzter, H., Kaduk, J., Tucker, C.J., 2015. Land degradation assessment using residual trend analysis of GIMMS NDVI3g, soil moisture and rainfall in Sub-Saharan West Africa from 1982 to 2012. Remote Sens. 7, 5471–5494. doi:10.3390/rs70505471

IPCC. Intergovernmenta Panel on Climate Change http://www.ipcc.ch/ipccreports/sres/land_use/index.php?idp=157. Accessed in oct-2018

Jacques, D.C., Kergoat, L., Hiernaux, P., Mougin, E., Defourny, P., 2014. Monitoring dry vegetation masses in semi-arid areas with MODIS SWIR bands. Remote Sens. Environ. 153, 40–49. doi:10.1016/j.rse.2014.07.027

Jamali, S., Jönsson, P., Eklundh, L., Ardö, J., Seaquist, J., 2015. Detecting changes in vegetation trends using time series segmentation. Remote Sens. Environ. 156, 182–195. doi:10.1016/j.rse.2014.09.010

Jin, C., Xiao, X., Merbold, L., Arneth, A., Veenendaal, E., Kutsch, W.L., 2013. Phenology and gross primary production of two dominant savanna woodland ecosystems in Southern Africa. Remote Sens. Environ. 135, 189–201. doi:10.1016/j.rse.2013.03.033

Ju, J., Masek, J.G., 2016. The vegetation greenness trend in Canada and US Alaska from

1984-2012 Landsat data. Remote Sensing of Environment. doi:10.1016/j.rse.2016.01.001

Karlson, M., Ostwald, M., 2016. Remote sensing of vegetation in the Sudano-Sahelian zone: A literature review from 1975 to 2014. J. Arid Environ. doi:10.1016/j.jaridenv.2015.08.022

Karnieli, A., Qin, Z., Wu, B., Panov, N., Yan, F., 2014. Spatio-temporal dynamics of land-use and land-cover in the Mu Us Sandy Land, China, using the change vector analysis technique. Remote Sens. 6, 9316–9339. doi:10.3390/rs6109316

Katsanos, D., Retalis, A., Michaelides, S., 2016. Validation of a high-resolution precipitation database (CHIRPS) over Cyprus for a 30-year period. Atmos. Res. 169, 459–464. doi:10.1016/j.atmosres.2015.05.015

Lambin, E.F., Geist, H.J., Lepers, E., 2003. Dynamics of land use and land cover change in tropical regions. Annu. Rev. Environ. Resour. 28, 205–241. doi:10.1146/annurev.energy.28.050302.105459

Lamchin, M., Lee, J.Y., Lee, W.K., Lee, E.J., Kim, M., Lim, C.H., Choi, H.A., Kim, S.R., 2016. Assessment of land cover change and desertification using remote sensing technology in a local region of Mongolia. Adv. Sp. Res. 57, 64–77. doi:10.1016/j.asr.2015.10.006

Le Toan, T., Quegan, S., Davidson, M.W.J., Balzter, H., Paillou, P., Papathanassiou, K., Plummer, S., Rocca, F., Saatchi, S., Shugart, H., Ulander, L., 2011. The BIOMASS mission: Mapping global forest biomass to better understand the terrestrial carbon cycle. Remote Sens. Environ. 115, 2850–2860. doi:10.1016/j.rse.2011.03.020

Leal, I.R., Da Silva, J.M.C., Tabarelli, M., Lacher, T.E., 2005. Changing the Course of Biodiversity Conservation in the Caatinga of Northeastern Brazil\rCambiando el Curso de la Conservación de Biodiversidad en la Caatinga del Noreste de Brasil. Conserv. Biol. 19, 701–706. doi:10.1111/j.1523-1739.2005.00703.x

Leroux, L., Bégué, A., Lo Seen, D., Jolivot, A., Kayitakire, F., 2017. Driving forces of recent vegetation changes in the Sahel: Lessons learned from regional and local level analyses. Remote Sens. Environ. 191, 38–54. doi:10.1016/j.rse.2017.01.014

Li, X.B., Li, R.H., Li, G.Q., Wang, H., Li, Z.F., Li, X., Hou, X.Y., 2016. Human-induced vegetation degradation and response of soil nitrogen storage in typical steppes in Inner Mongolia, China. Journal of Arid Environments. doi:10.1016/j.jaridenv.2015.07.013

Lima, A.L.A., Rodal, M.J.N., 2010. Phenology and wood density of plants growing in the semi-arid region of northeastern Brazil, Journal of Arid Environments. doi:10.1016/j.jaridenv.2010.05.009

Lima, G.D.S., Lima, J.R. de F., Silva, N. da, Oliveira, R.S. de, Lucena, R.F.P., 2016. Inventory in situ of plant resources used as fuel in the Semiarid Region of Northeast Brazil. Brazilian J. Biol. Sci. 3, 45. doi:10.21472/bjbs.030505

Linares-Palomino, R., Oliveira-Filho, A.T., Pennington, R.T., 2011. Seasonally Dry Tropical Forests 3–21. doi:10.5822/978-1-61091-021-7

Liu, F., Chen, Y., Lu, H., Shao, H., 2017. Albedo indicating land degradation around the Badain Jaran Desert for better land resources utilization. Sci. Total Environ. 578, 67–73. doi:10.1016/j.scitotenv.2016.06.171

Loveland, T.R., Dwyer, J.L., 2012. Landsat: Building a strong future. Remote Sensing of Environment. 122, 22–29. doi:10.1016/j.rse.2011.09.022

Marengo, J.A., Torres, R.R., Alves, L.M., 2017. Drought in Northeast Brazil—past, present, and future. Theor. Appl. Climatol. 129, 1189–1200. doi:10.1007/s00704-016-1840-8

Mariano, D.A., Santos, C.A.C. do., Wardlow, B.D., Anderson, M.C., Schiltmeyer, A. V., Tadesse, T., Svoboda, M.D., 2018. Use of remote sensing indicators to assess effects of drought and human-induced land degradation on ecosystem health in Northeastern Brazil. Remote Sens. Environ. 213, 129–143. doi:10.1016/j.rse.2018.04.048

Mas, 1999. International Journal of Monitoring land-cover changes : A comparison of change detection techniques. Int. J. Remote Sens. 20, 139–152. doi:10.1080/014311699213659

Masek, J.G., Vermote, E.F., Saleous, N.E., Wolfe, R., Hall, F.G., Huemmrich, K.F., Gao, F., Kutler, J., Lim, T., 2006. A Landsat Surface Reflectance Dataset for North America, 1990–2000. IEEE Geoscience and Remote Sensing Letters, 3(1), 68–72. doi:10.1109/lgrs.2005.857030

Mayes, M.T., Mustard, J.F., Melillo, J.M., 2015. Forest cover change in Miombo Woodlands: Modeling land cover of African dry tropical forests with linear spectral mixture analysis. Remote Sens. Environ. 165, 203–215. doi:10.1016/j.rse.2015.05.006

Medeiros, I.C., da Costa Silva, J.F.C.B., Silva, R.M., Santos, C.A.G., 2018. Run-off–erosion modelling and water balance in the Epitácio Pessoa Dam river basin, Paraíba State in Brazil. Int. J. Environ. Sci. Technol. doi:10.1007/s13762-018-1940-3

MMA, Brazilian Ministry of the Environment, 2018. http://geocatalogo.mma.gov.br/

Moro, M.F., Lughadha, E.N., Araújo, F.S. De, Martins, F.R., 2016. A Phytogeographical Metaanalysis of the Semiarid Caatinga Domain in Brazil. Bot. Rev. doi:10.1007/s12229-016-9164-z

Munyati, C., Mboweni, G., 2013. Variation in NDVI values with change in spatial resolution for semi-arid savanna vegetation: A case study in northwestern South Africa. Int. J. Remote Sens. 34, 2253–2267. doi:10.1080/01431161.2012.743692

Nagler, P.L., Daughtry, C.S.T., Goward, S.N., 2000. Plant litter and soil reflectance. Remote Sens. Environ. 71, 207–215. doi:10.1016/S0034-4257(99)00082-6

National Institute of Meteorology of Brazil, 2018. Available: http://www.inmet.gov.br/portal/index.php?r=bdmep/bdmep

Paredes-Trejo, F.J., Barbosa, H.A., Lakshmi Kumar, T. V., 2017. Validating CHIRPS-based satellite precipitation estimates in Northeast Brazil. J. Arid Environ. 139, 26–40. doi:10.1016/j.jaridenv.2016.12.009

Pereira, I.M., Andrade, L.A., Sampaio, E.V.S.B., Barbosa, M.R. V., 2003. Use-history Effects on Structure and Flora of Caatinga. Biotropica 35, 154–165. doi:10.1111/j.1744-7429.2003.tb00275.x

Pinheiro, E.A.R., Costa, C.A.G., De Araújo, J.C., 2013. Effective root depth of the Caatinga biome. J. Arid Environ. 89, 1–4. doi:10.1016/j.jaridenv.2012.10.003

R Core Team, 2017. R: A language and environment for statistical computing. R Foundation for Statistical Computing, Vienna, Austria. URL https://www.R-project.org/.

Rodal, M., Barbosa, M., Thomas, W., 2008. Do the seasonal forests in northeastern Brazil represent a single floristic unit? Brazilian J. Biol. 68, 467–475. doi:10.1590/S1519-69842008000300003

Rodríguez-Caballero, E., Knerr, T., Weber, B., 2015. Importance of biocrusts in dryland monitoring using spectral indices. Remote Sens. Environ. 170, 32–39.

doi:10.1016/j.rse.2015.08.034

Saco, P.M., Moreno-de las Heras, M., Keesstra, S., Baartman, J., Yetemen, O., Rodríguez, J.F., 2018. Vegetation and soil degradation in drylands: Non linear feedbacks and early warning signals. Curr. Opin. Environ. Sci. Heal. 5, 67–72. doi:10.1016/j.coesh.2018.06.001

Salcedo, I.H., Tiessen, H., Sampaio, E.V.S.B., 1997. Nutrient availability in, soil samples from shifting cultivation sites in the semi-arid Caatinga of NE Brazil. Agric. Ecosyst. Environ. 65, 177–186. doi:10.1016/S0167-8809(97)00073-X

Samain, O., Kergoat, L., Hiernaux, P., Guichard, F., Mougin, E., Timouk, F., Lavenu, F., 2008. Analysis of the in situ and MODIS albedo variability at multiple timescales in the sahel. J. Geophys. Res. Atmos. 113, 1–16. doi:10.1029/2007JD009174

Santos, a M., Tabarelli, M., 2002. Distance from roads and cities as a predictor of habitat loss and fragmentation in the caatinga vegetation of Brazil. Braz. J. Biol. 62, 897–905. doi:10.1590/S1519-69842002000500020

Santos, R.M., Oliveira-Filho, A.T., Eisenlohr, P. V., Queiroz, L.P., Cardoso, D.B.O.S., Rodal, M.J.N., 2012. Identity and relationships of the Arboreal Caatinga among other floristic units of seasonally dry tropical forests (SDTFs) of north-eastern and Central Brazil, Ecology and Evolution. doi:10.1002/ece3.91

Savitzky, A., Golay, M.J.E., 1964. Smoothing and Differentiation of Data by Simplified Least Squares Procedures. Anal. Chem. 36, 1627–1639. doi:10.1021/ac60214a047

Schertz, T., Alexander, R., Ohe, D., 1991. The computer program Estimate Trend (ESTREND), a system for the Detection of Trends in Water-quality data 1–63.

Schucknecht, A., Erasmi, S., Niemeyer, I., Matschullat, J., 2013. Assessing vegetation variability and trends in north-eastern Brazil using AVHRR and MODIS NDVI time series. European Journal of Remote Sensing. 46, 40–59. doi:10.5721/EuJRS20134603

Shuai, Y., Masek, J.G., Gao, F., Schaaf, C.B., 2011. An algorithm for the retrieval of 30-m snow-free albedo from Landsat surface reflectance and MODIS BRDF. Remote Sens. Environ. 115, 2204–2216. doi:10.1016/j.rse.2011.04.019

Shuai, Y., Masek, J.G., Gao, F., Schaaf, C.B., He, T., 2014. An approach for the long-term 30-m land surface snow-free albedo retrieval from historic Landsat surface reflectance and MODIS-based a priori anisotropy knowledge. Remote Sens. Environ. 152, 467–479. doi:10.1016/j.rse.2014.07.009

Silva, G.C., Sampaio, E.V.S.B., 2008. Biomassas de partes aéreas em plantas da Caatinga. Soc. Investig. Florestais 32, 567–575. doi:10.1016/j.jaridenv.2015.02.003

Sobrinho, M. S., Tabarelli, M. , Machado, I. C., Sfair, J. C., Bruna, E. M. and Lopes, A. V. 2016. Land use, fallow period and the recovery of a Caatinga forest. Biotropica, 48:586-597. doi:10.1111/btp.12334

Song, X.P., Huang, C., Sexton, J.O., Channan, S., Townshend, J.R., 2014. Annual detection of forest cover loss using time series satellite measurements of percent tree cover. Remote Sensing. 6, 8878–8903. doi:10.3390/rs6098878

Stroppiana, D., Bordogna, G., Carrara, P., Boschetti, M., Boschetti, L., Brivio, P.A., 2012. A method for extracting burned areas from Landsat TM/ETM+ images by soft aggregation of multiple Spectral Indices and a region growing algorithm. ISPRS J. Photogramm. Remote Sens. 69, 88–102. doi:10.1016/j.isprsjprs.2012.03.001

Torrence, C., Compo, G.P., 1998. A practical guide to wavelet analysis. Bull. Am. Meteor. Soc. 79, 61–78. doi:10.1175/1520-0477(1998)079<0061:APGTWA>2.0.CO;2

Tucker, C.J., 1979. Red and photographic infrared linear combinations for monitoring vegetation. Remote Sens. Environ. 8, 127–150. doi:10.1016/0034-4257(79)90013-0

U.S. Geological Survey, 2018a. Product Guide: LANDSAT 4-7 SURFACE REFLECTANCE (LEDAPS) PRODUCT. Department of the Interior Version 8.3, https://landsat.usgs.gov/sites/default/files/documents/ledaps_product_guide.pdf

U.S. Geological Survey, 2018b. Product Guide: Landsat 8 Surface Reflectance code (LaSRC) product. Department of the Interior Version 4.3, https://landsat.usgs.gov/sites/default/files/documents/lasrc_product_guide.pdf

Verbesselt, J., Hyndman, R., Newnham, G., Culvenor, D., 2010. Detecting trend and seasonal changes in satellite image time series. Remote Sens. Environ. doi:10.1016/j.rse.2009.08.014

Verbesselt, J., Umlauf, N., Hirota, M., Holmgren, M., Van Nes, E.H., Herold, M., Zeileis, A., Scheffer, M., 2016. Remotely sensed resilience of tropical forests. Nat. Clim. Chang. doi:10.1038/nclimate3108

Verbesselt, J., Zeileis, A., Herold, M., 2012. Near real-time disturbance detection using satellite image time series. Remote Sens. Environ. doi:10.1016/j.rse.2012.02.022

Vermote, E., Justice, C., Claverie, M., Franch, B., 2016. Remote Sensing of Environment Preliminary analysis of the performance of the Landsat 8 / OLI land surface reflectance product. Remote Sens. Environ. doi:10.1016/j.rse.2016.04.008

Vicente-Serrano S.M., Beguería, S. López-Moreno, J.I., 2010. A Multi-scalar drought index sensitive to global warming: The Standardized Precipitation Evapotranspiration Index - SPEI. Journal of Climate 23, 1696-1718. https://doi.org/10.1175/2009JCLI2909.1

Walker, J., de Beurs, K., Wynne, R.H., 2015. Phenological response of an Arizona dryland forest to short-term climatic extremes. Remote Sens. 7, 10832–10855. doi:10.3390/rs70810832

Wang, Z., Erb, A.M., Schaaf, C.B., Sun, Q., Liu, Y., Yang, Y., Shuai, Y., Casey, K.A., Román, M.O., 2016. Remote Sensing of Environment Early spring post- fi re snow albedo dynamics in high latitude boreal forests using Landsat-8 OLI data. Remote Sens. Environ. 185, 71–83. doi:http://dx.doi.org/10.1016/j.rse.2016.02.059

Wang, Z., Schaaf, C.B., Sun, Q., Kim, J., Erb, A.M., Gao, F., Román, M.O., Yang, Y., Petroy, S., Taylor, J.R., Masek, J.G., Morisette, J.T., Zhang, X., Papuga, S.A., 2017. Monitoring land surface albedo and vegetation dynamics using high spatial and temporal resolution synthetic time series from Landsat and the MODIS BRDF/NBAR/albedo product. International Journal of Applied Earth Observation and Geoinformation. doi:10.1016/j.jag.2017.03.008

Wessels, K.J., Prince, S.D., Malherbe, J., Small, J., Frost, P.E., VanZyl, D., 2007. Can human-induced land degradation be distinguished from the effects of rainfall variability? A case study in South Africa. J. Arid Environ. 68, 271–297. doi:10.1016/j.jaridenv.2006.05.015

Wessels, K.J., van den Bergh, F., Scholes, R.J., 2012. Limits to detectability of land degradation by trend analysis of vegetation index data. Remote Sens. Environ. 125, 10–22. doi:10.1016/j.rse.2012.06.022

Wulder, M.A., White, J.C., Loveland, T.R., Woodcock, C.E., Belward, A.S., Cohen, W.B., Fosnight, E.A., Shaw, J., Masek, J.G., Roy, D.P., 2016. The global Landsat archive:

Status, consolidation, and direction. Remote Sensing of Environment. 185, 271–283. doi:10.1016/j.rse.2015.11.032

Xu, D., Guo, X., Li, Z., Yang, X., Yin, H., 2014. Remote Sensing of Environment Measuring the dead component of mixed grassland with Landsat imagery. Remote Sens. Environ. 142, 33–43. doi:10.1016/j.rse.2013.11.017

Yang, Y., Wang, Z., Li, J., Gang, C., Zhang, Y., Zhang, Y., Odeh, I., Qi, J., 2016. Comparative assessment of grassland degradation dynamics in response to climate variation and human activities in China, Mongolia, Pakistan and Uzbekistan from 2000 to 2013. Journal of Arid Environments. 135, 164–172. doi:10.1016/j.jaridenv.2016.09.004

Yu, Y., Notaro, M., Wang, F., Mao, J., Shi, X., Wei, Y., 2017. Observed positive vegetation-rainfall feedbacks in the Sahel dominated by a moisture recycling mechanism. Nat. Commun. 8, 1–9. doi:10.1038/s41467-017-02021-1

Zhang, J., Niu, J.M., Bao, T., Buyantuyev, A., Zhang, Q., Dong, J.J., Zhang, X.F., 2014. Human induced dryland degradation in Ordos Plateau, China, revealed by multilevel statistical modeling of normalized difference vegetation index and rainfall time-series. J. Arid Land 6, 219–229. doi:10.1007/s40333-013-0203-x

Zhao, Y., Wang, X., Novillo, C.J., Arrogante-Funes, P., Vázquez-Jiménez, R., Maestre, F.T., 2018. Albedo estimated from remote sensing correlates with ecosystem multifunctionality in global drylands. J. Arid Environ. 157, 116–123. doi:10.1016/j.jaridenv.2018.05.010